

Supplementary Information

Edge State Wave Functions from Momentum-Conserving Tunneling Spectroscopy

T. Patlatiuk,^{1,*} C.P. Scheller,^{1,*} D. Hill,² Y. Tserkovnyak,² J. C. Egues,³ G.
Barak,⁴ A. Yacoby,⁴ L. N. Pfeiffer,⁵ K. W. West,⁵ and D. M. Zumbühl^{1,†}

¹*Departement Physik, University of Basel,
Klingelbergstrasse 82, CH-4056 Basel, Switzerland*

²*Department of Physics and Astronomy,
University of California, Los Angeles, California 90095, USA*

³*Instituto de Física de São Carlos, Universidade de São Paulo,
13560-970 São Carlos, São Paulo, Brazil*

⁴*Department of Physics, Harvard University,
Cambridge, Massachusetts 02138, USA*

⁵*Department of Electrical Engineering,
Princeton University, Princeton, New Jersey 08544, USA*

* equally contributing authors

† dominik.zumbuhl@unibas.ch

CONTENTS

I. Measurement configuration and sample misalignment correction	1
II. Tunneling between numerous hybrid states and lower wire modes	3
A. Tunneling from H_0	3
B. Tunneling into LW_1	5
C. Tunneling into LW_2	7
D. Tunneling into LW_3	8
E. Tunneling into LW_4	9
F. Tunneling into LW_5	10
III. Interpretation of the tunneling signal	11
IV. Exception from the selection rule	13
V. Hybridization	14
VI. Electron density profiles	15
VII. Numerical calculations	16
References	17

I. MEASUREMENT CONFIGURATION AND SAMPLE MISALIGNMENT CORRECTION

The surface gate was used to deplete the 2DEG and the upper wire underneath it, forcing electrons from the source ohmic contact to propagate through the 2DEG region, tunnel to the lower wire, propagate along the lower wire under the gate and tunnel to the 2DEG connected to the drain on the other side of the gate. All the measurements presented in this paper were done with a small AC excitation (lock-in technique) at zero DC bias, ensuring that tunneling takes place only between states close to the Fermi level. Microwave filters and thermalizers [1–3] on each lead provide an electron temperature around 10 mK, see [4] for details.

A small misalignment of the sample coordinate system from the axis of the vector magnet was corrected using a rotation matrix. A rotation around the x -axis shown in Fig.S1(a) by an angle $\alpha = -3.5^\circ$ explains the measured Hall voltages (recorded with deenergized gates) induced by magnets pointing along Y' and Z' directions. Such a rotation around only one axis by a rather small angle is the simplest alignment correction consistent with the measured out-of-plane components. The conductance value $g(B_Y, B_Z)$ in the sample coordinate system, see panel Fig.S1(c), was obtained using linear interpolation among the four nearest measurement points from Fig.S1(b) with coordinates $(B_{Y'}, B_{Z'})$ given by:

$$\begin{pmatrix} B_{Y'} \\ B_{Z'} \end{pmatrix} = \begin{pmatrix} \cos(\alpha) & \sin(\alpha) \\ -\sin(\alpha) & \cos(\alpha) \end{pmatrix} \begin{pmatrix} B_Y \\ B_Z \end{pmatrix}$$

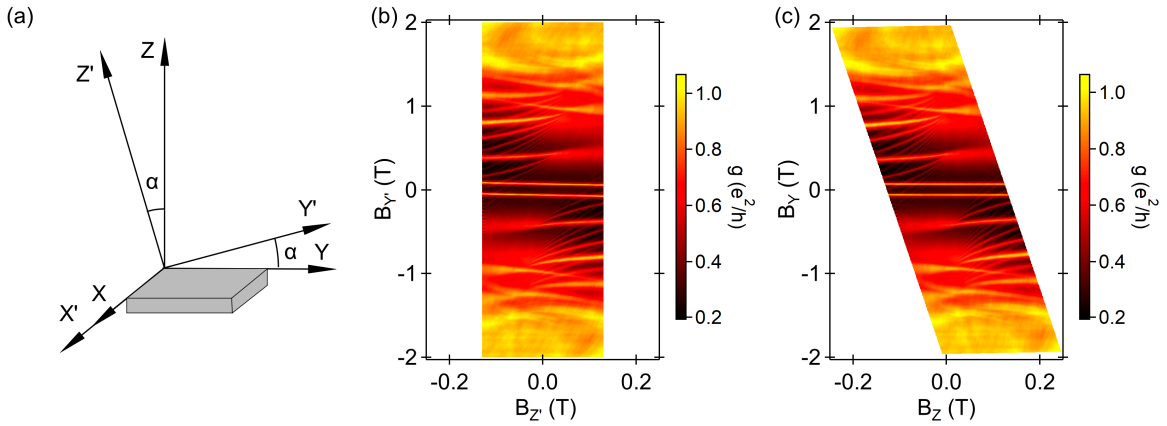


FIG. S1. (a) The magnet axis ($X'Y'Z'$) and the sample axis (XYZ). (b) Conductance measurements in the original basis (magnet axis). (c) Conductance measurements after correcting for the sample misalignment.

II. TUNNELING BETWEEN NUMEROUS HYBRID STATES AND LOWER WIRE MODES

The regions of substantial spatial overlap between hybrid state and lower wire wave functions are highlighted with dashed rectangles in Fig. S2, Fig. S3, Fig. S5–Fig. S8. The top and bottom boundaries of these rectangles are defined as the lines for which the normalized wave functions drop below a small predefined value, here 5×10^{-4} . The left and right boundaries are defined in a similar way by the more narrow wave function of the two in the y -direction. The pair of wave functions with the strongest overlap for a given magnetic field B_Z (row) is highlighted with a dashed green rectangle in Fig. S3, Fig. S5–Fig. S8.

A. Tunneling from H_0

The wave function of the hybrid state H_0 and lower wire modes LW_2 , LW_3 , LW_4 , and LW_5 matched in k_x -momenta by the magnetic field B_Y are shown in the first, second, third, and fourth columns in Fig. S2. The square of the wave function overlap normalized to its global maximum value in Fig. 2(c) of the main text is indicated as a numeric value in each panel. Tunneling to wire modes $LW_{2,3,4,5}$ is strongly suppressed due to wave function orthogonality. In contrast, the normalized overlap between H_0 and the lower wire mode LW_1 reaches the maximal value of 1. Corresponding wave functions are shown in the first column in Fig. S3.

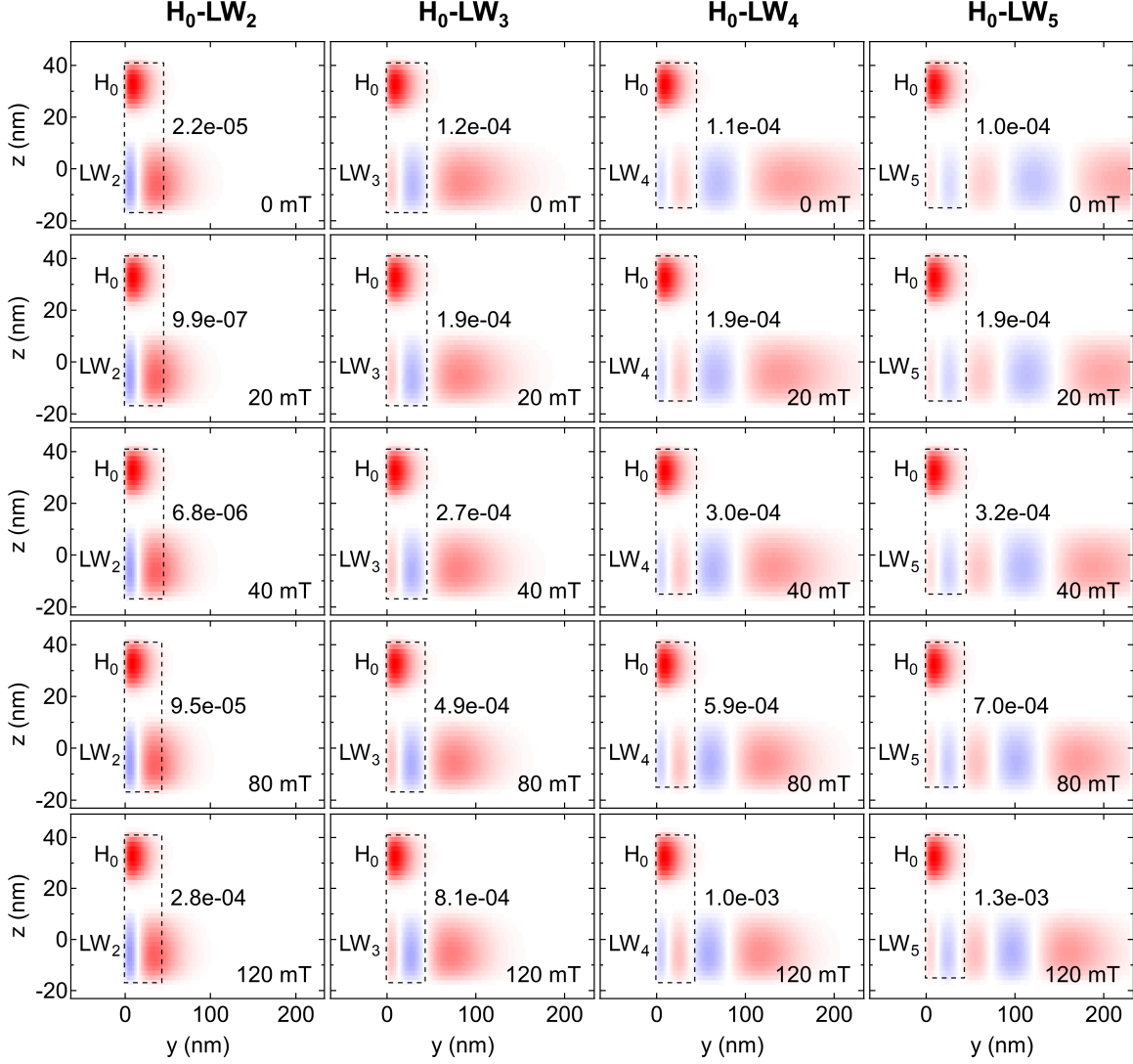


FIG. S2. The wave function of the hybrid state H_0 in the upper quantum well brought into resonance with the lower wire modes LW_2 , LW_3 , LW_4 and LW_5 calculated for a number of magnetic field values B_Z as indicated. The dashed rectangle highlights the regions of substantial overlap between the wave functions. The square of the wave function overlap normalized to its global maximum in Fig. 2(c) of the main text is indicated as a numeric value in each panel. None of the rectangles is highlighted in green, as all these resonances are very weak.

B. Tunneling into LW_1

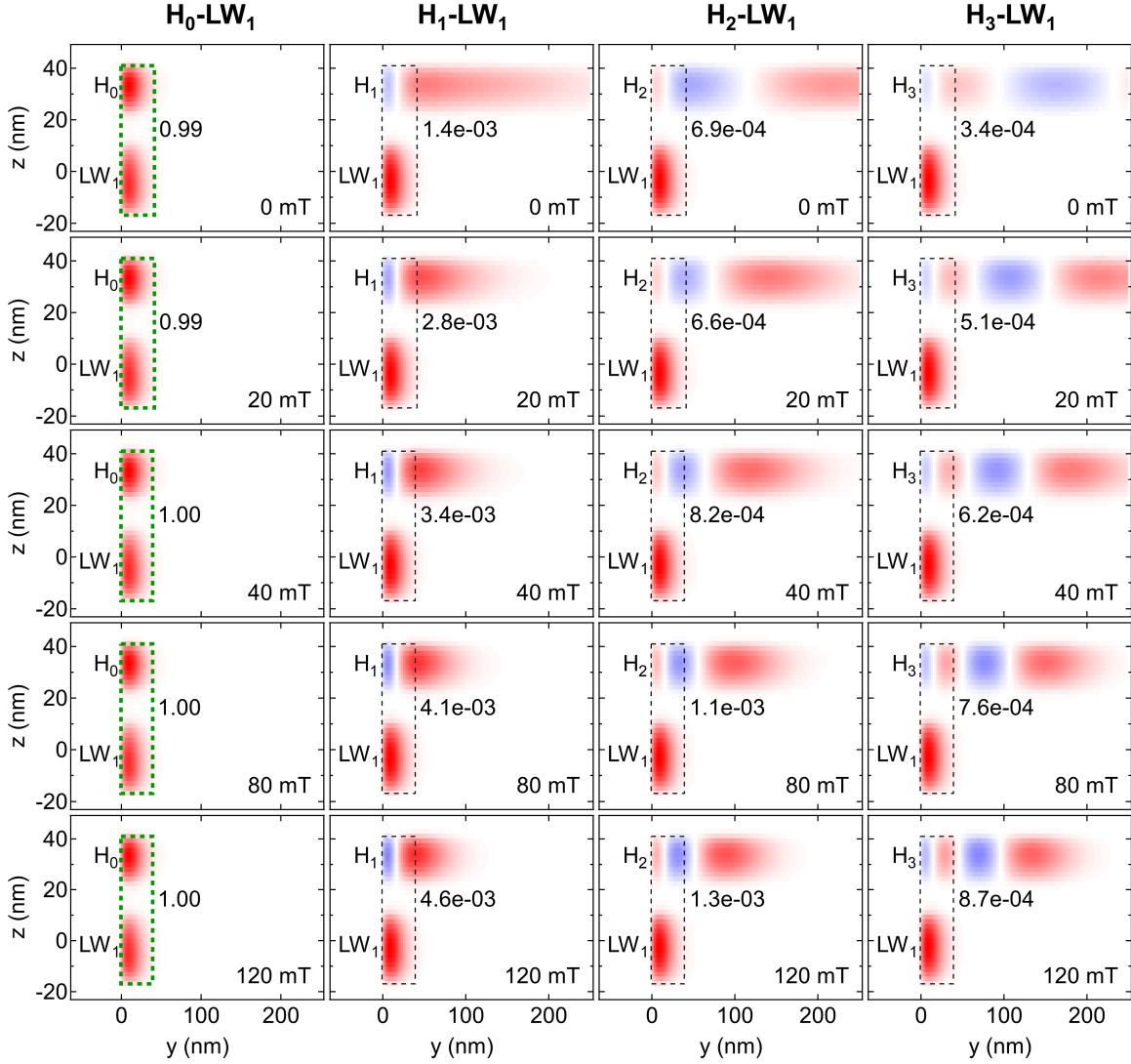


FIG. S3. The wave function of the hybrid states H_0 , H_1 , H_2 , H_3 , and wire mode LW_1 calculated for a number of perpendicular magnetic field values B_Z as indicated. The dashed rectangle highlights the regions of substantial overlap between the wave functions. The square of the wave function overlap normalized to its global maximum in Fig. 2(c) of the main text is indicated as a numeric value in each panel. The pair of wave functions with the strongest overlap for a given magnetic field B_Z (row) is highlighted with a green color.

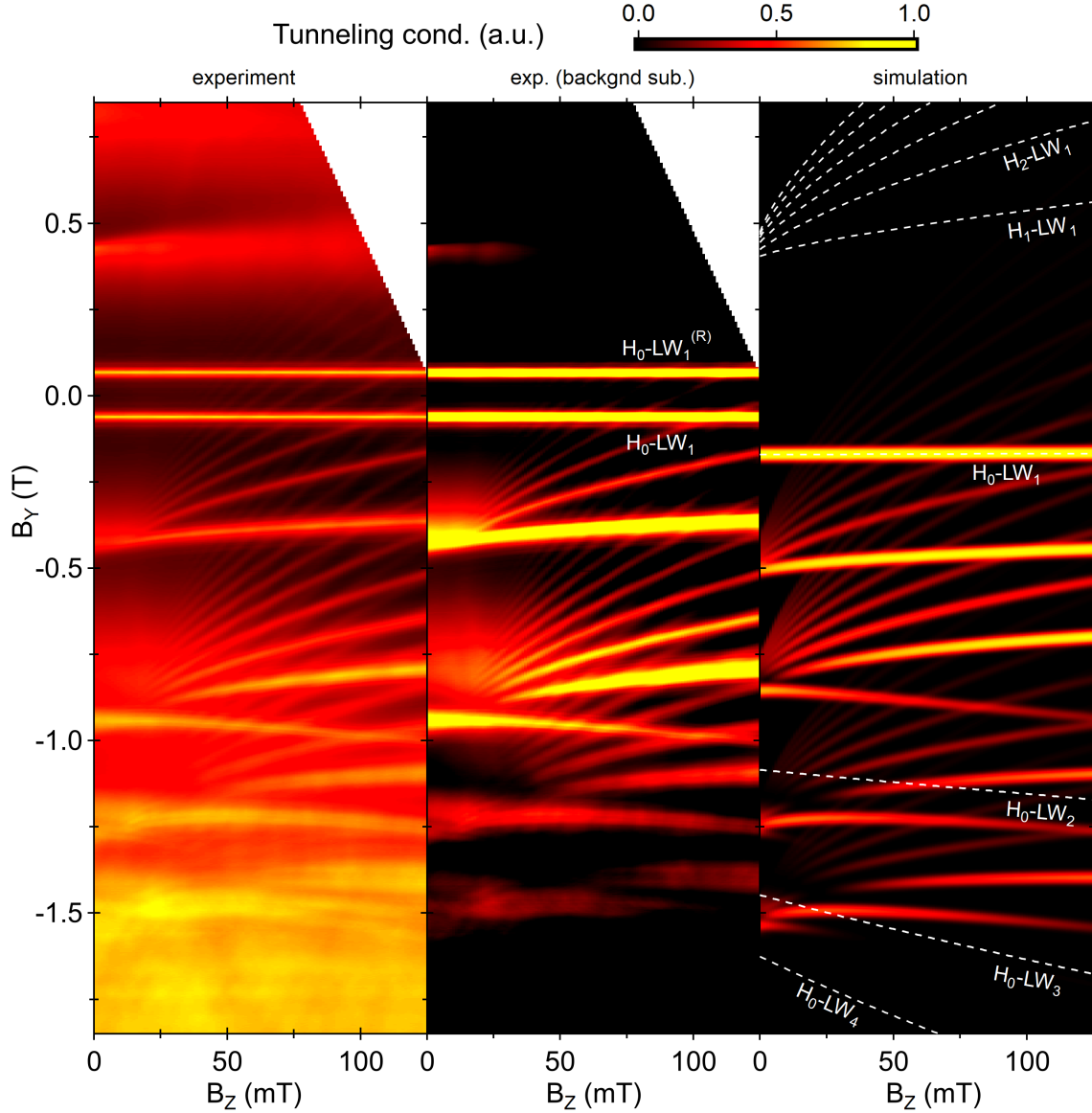


FIG. S4. The normalized tunneling conductance with (left) and without (middle) the smoothly varying background. The range of the magnetic field B_Y is wider compared to Fig. 2 of the main text. The calculated tunneling conductance to the lower wire modes $LW_{1,2,3,4,5}$ is shown in the right panel. The tunneling to the lower wire mode LW_1 is very weak for all the hybrid states except H_0 . The white dashed curves at the top of the right panel indicate the predicted position of the resonances $H_1 - LW_1, H_2 - LW_1, \dots$. Three dashed curves at the bottom of the right panel indicate the predicted position of the suppressed resonances $H_0 - LW_2, H_0 - LW_3$, and $H_0 - LW_4$ (see Fig. S2 for details). In agreement with the simulations, all the resonances marked with the dashed curves are not observed in the measurements (left and middle panels). More work would be required to understand the comparatively large broadening of the $LW_{4,5}$ resonances, or to capture better the magnetic field B_Z where orthogonality to $LW_{3,4,5}$ is observed.

C. Tunneling into LW_2

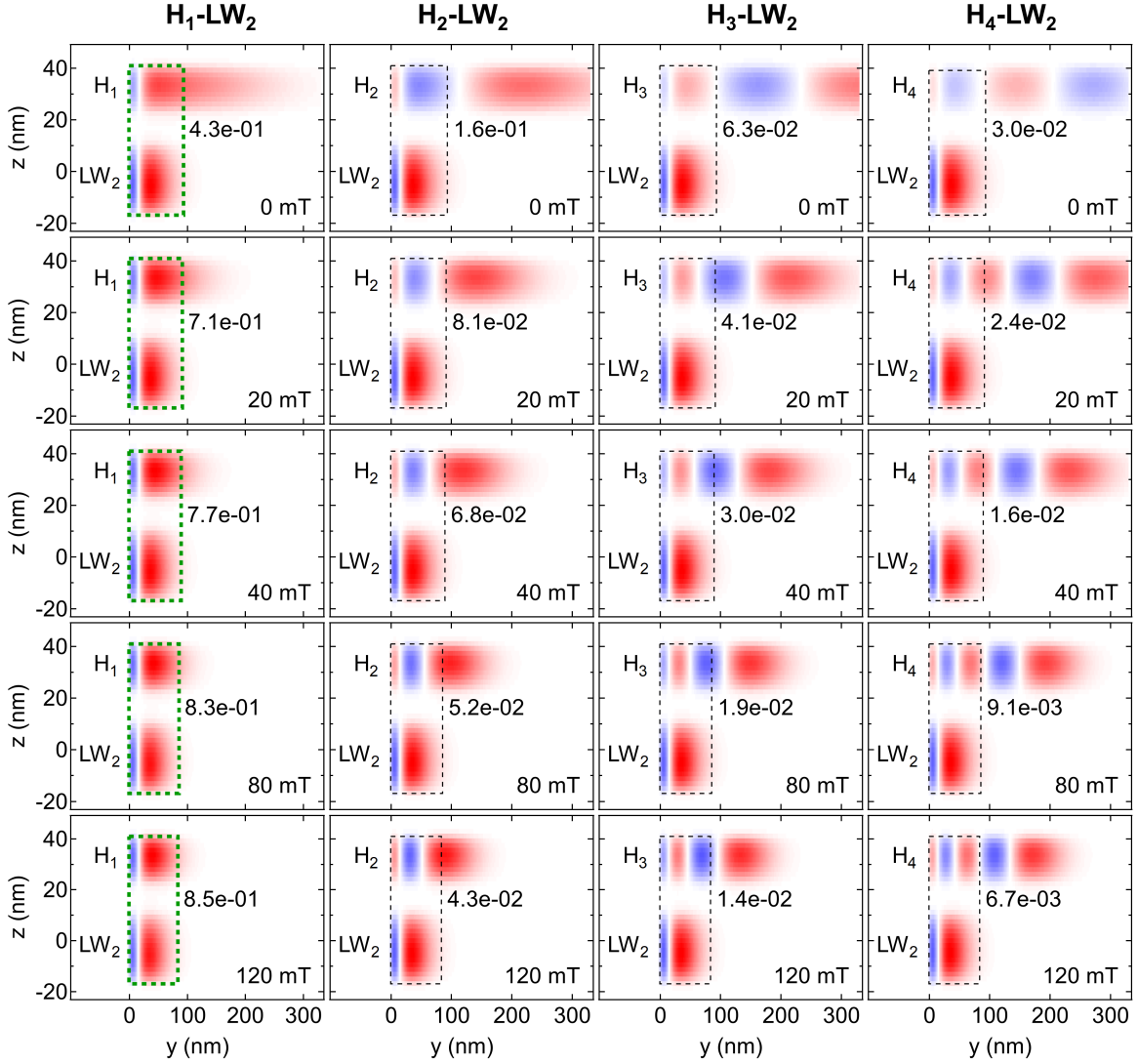


FIG. S5. The wave function of the hybrid states H_1 , H_2 , H_3 , H_4 , and wire mode LW_2 calculated for a number of perpendicular magnetic field values B_Z as indicated. The dashed rectangle highlights the regions of substantial overlap between the wave functions. The square of the wave function overlap normalized to its global maximum in Fig. 2(c) of the main text is indicated as a numeric value in each panel. The pair of wave functions with the strongest overlap for a given magnetic field B_Z (row) is highlighted with a green color.

D. Tunneling into LW_3

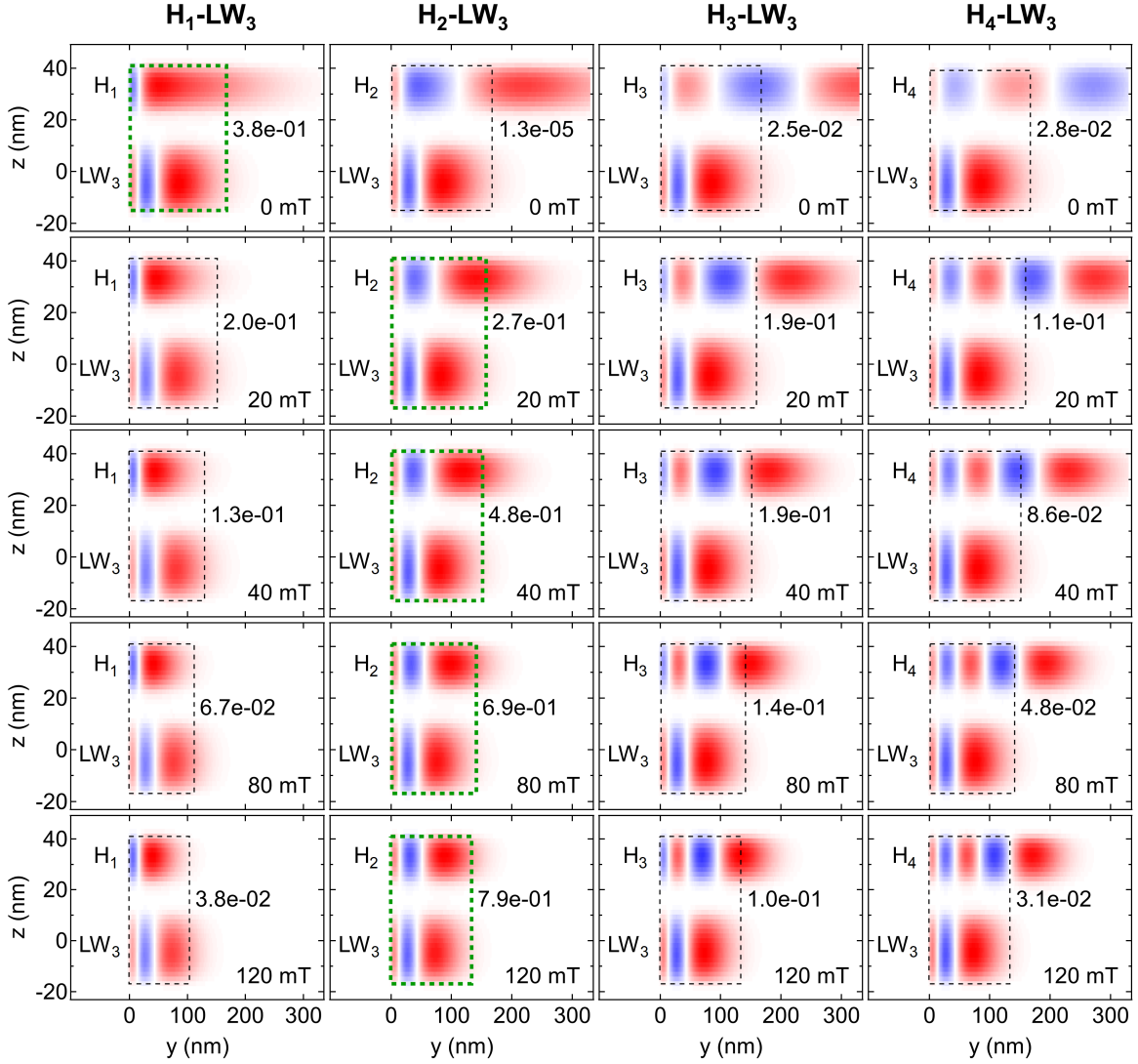


FIG. S6. The wave function of the hybrid states H_1, H_2, H_3, H_4 , and wire mode LW_3 calculated for a number of perpendicular magnetic field values B_Z as indicated. The dashed rectangle highlights the regions of substantial overlap between the wave functions. The square of the wave function overlap normalized to its global maximum in Fig. 2(c) of the main text is indicated as a numeric value in each panel. The pair of wave functions with the strongest overlap for a given magnetic field B_Z (row) is highlighted with a green color.

E. Tunneling into LW_4

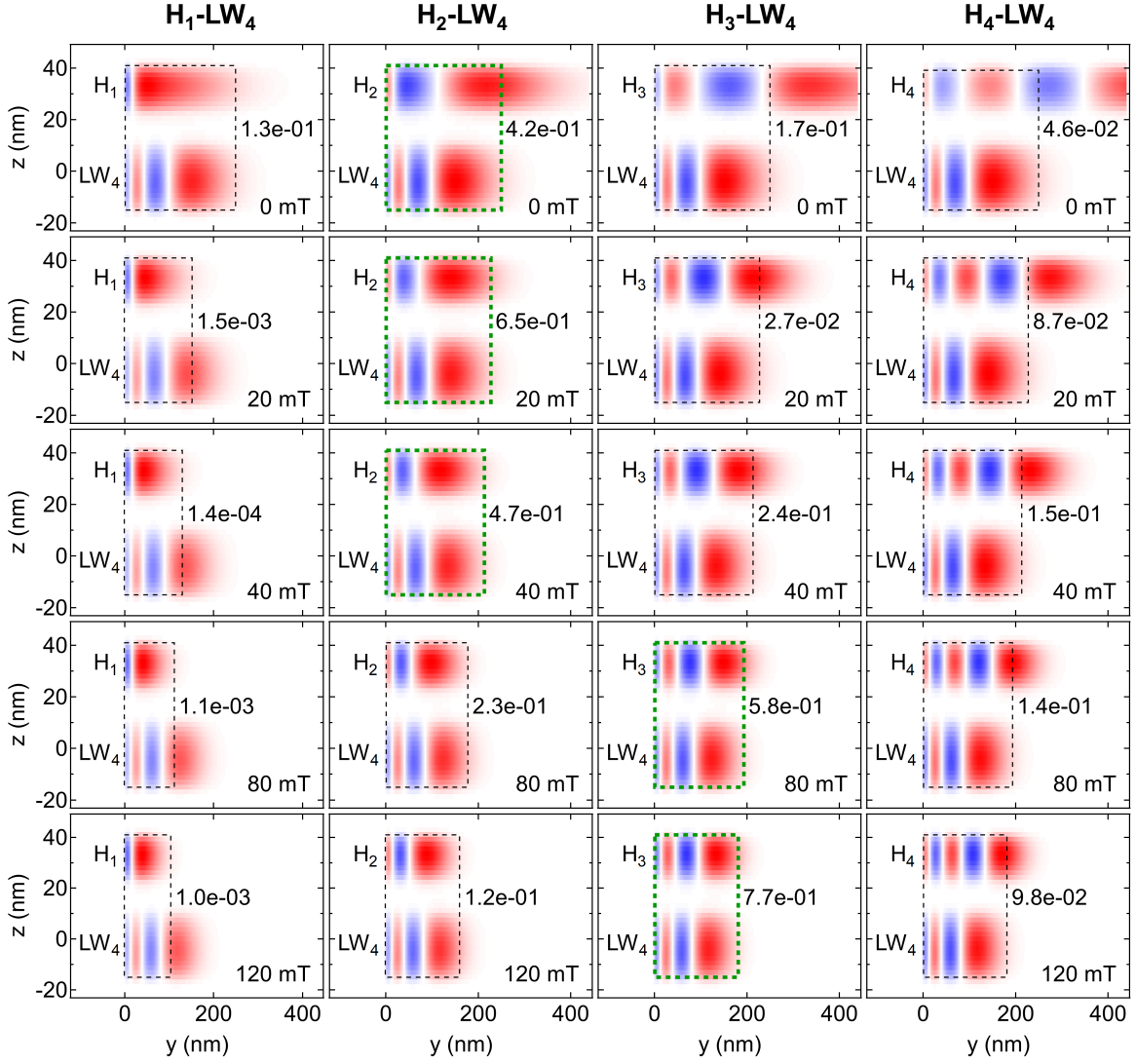


FIG. S7. The wave function of the hybrid states H_1 , H_2 , H_3 , H_4 , and wire mode LW_4 calculated for a number of perpendicular magnetic field values B_Z as indicated. The dashed rectangle highlights the regions of substantial overlap between the wave functions. The square of the wave function overlap normalized to its global maximum in Fig. 2(c) of the main text is indicated as a numeric value in each panel. The pair of wave functions with the strongest overlap for a given magnetic field B_Z (row) is highlighted with a green color.

F. Tunneling into LW_5

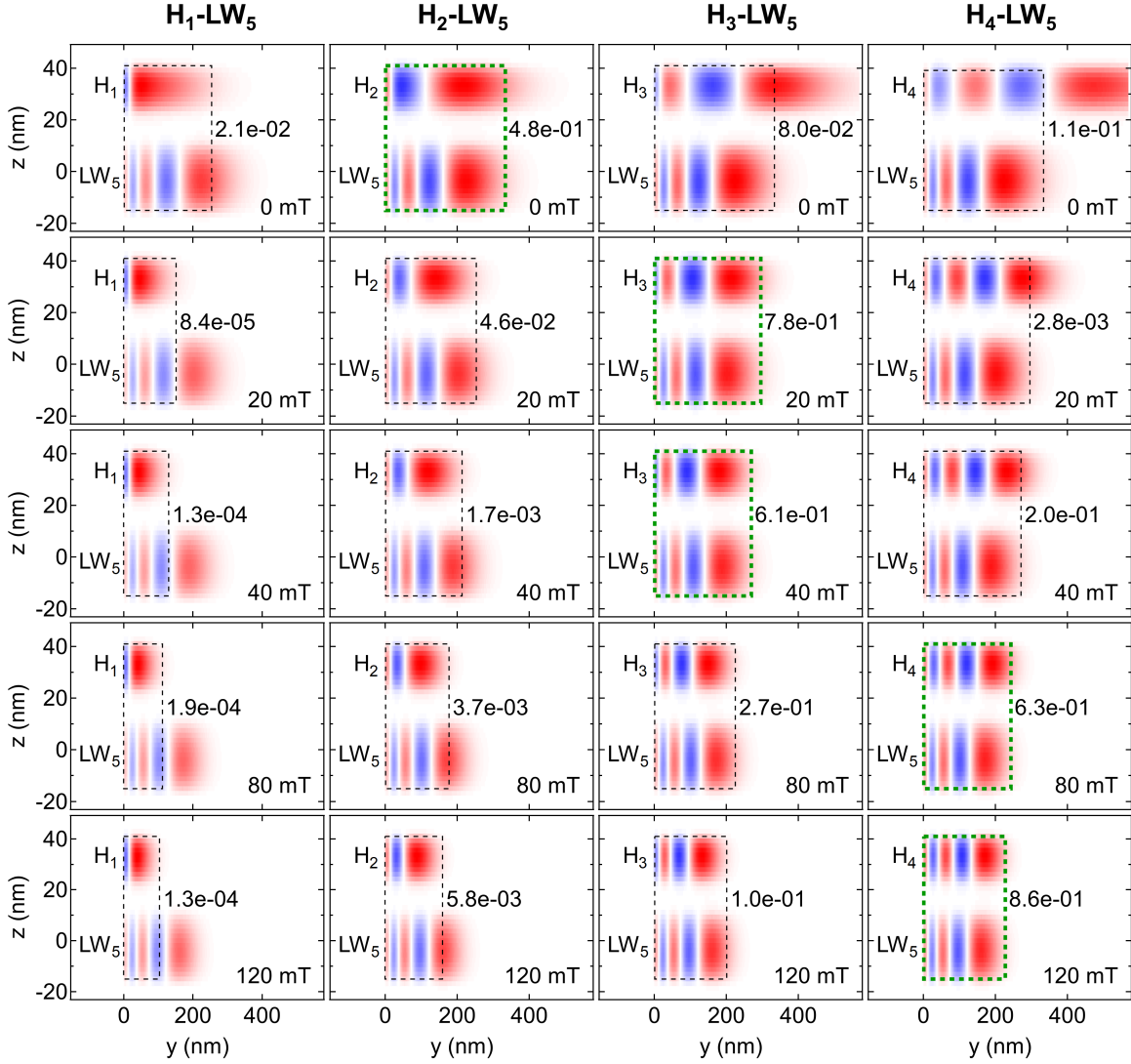


FIG. S8. The wave function of the hybrid states H_1 , H_2 , H_3 , H_4 , and wire mode LW_5 calculated for a number of perpendicular magnetic field values B_Z as indicated. The dashed rectangle highlights the regions of substantial overlap between the wave functions. The square of the wave function overlap normalized to its global maximum in Fig. 2(c) of the main text is indicated as a numeric value in each panel. The pair of wave functions with the strongest overlap for a given magnetic field B_Z (row) is highlighted with a green color.

III. INTERPRETATION OF THE TUNNELING SIGNAL

To visualize the origin of tunneling conductance variations we plot the wave function cross sections along the y -direction for $z = 0$ (upper system) and $z = 31$ nm (lower system), Fig. S9(a,b), corresponding to the center of the upper and lower quantum wells, respectively. Solid curves correspond to the cross sections of the hybrid states H_1 (panel a) and H_2 (panel b), while dashed curves correspond to the cross section of the wave function of the lower wire LW_3 . The values of the magnetic field B_Z are labeled and color coded.

At zero magnetic field, the comparably soft upper system confinement potential forms a strongly asymmetric wave function of the hybrid state H_1 which has only one node (solid red curve). The strong and wide second lobe of this wave function protrudes deeply into the bulk of the sample. As the magnetic field B_Z is increased, the width of this lobe reduces significantly. In contrast, the wave function of the lower wire mode LW_3 is modified only slightly by magnetic field, due to the stronger triangular confinement potential along the y -direction in the lower system, see Fig. 1(c) in the main text.

The exponential decay of the wave function inside the AlGaAs barrier as well as the wave function profiles in the y -direction determine the strength of the overlap, given by the product of the y -wave function profiles in upper and lower system, shown in panel (c). The products integrated along the y -direction are shown in panel (e). At $B_Z = 0$ (red) the product of the wave function profiles has two small negative lobes and one wide positive lobe, which dominates the integrated value. As the magnetic field B_Z is increased, the strength of the negative lobes is increased. At the same time, the width of the positive lobe is reduced. As a consequence, the result of the integration that is directly related to the wave function overlap is also reduced. This explains the reduction of the tunneling conductance of the $H_1 - LW_3$ resonance as the magnetic field B_Z increases.

The right column of Fig. S9 shows the wave functions (b), their products (d), and result of integration for the hybrid state H_2 and lower wire mode LW_3 . In this case, the small overlap at small B_Z is caused by different length scale of the wave functions that becomes comparable at higher fields. As a consequence, the tunneling conductance of the $H_2 - LW_3$ resonance is very small at small B_Z and rapidly increases in the presence of magnetic field along the z -direction.

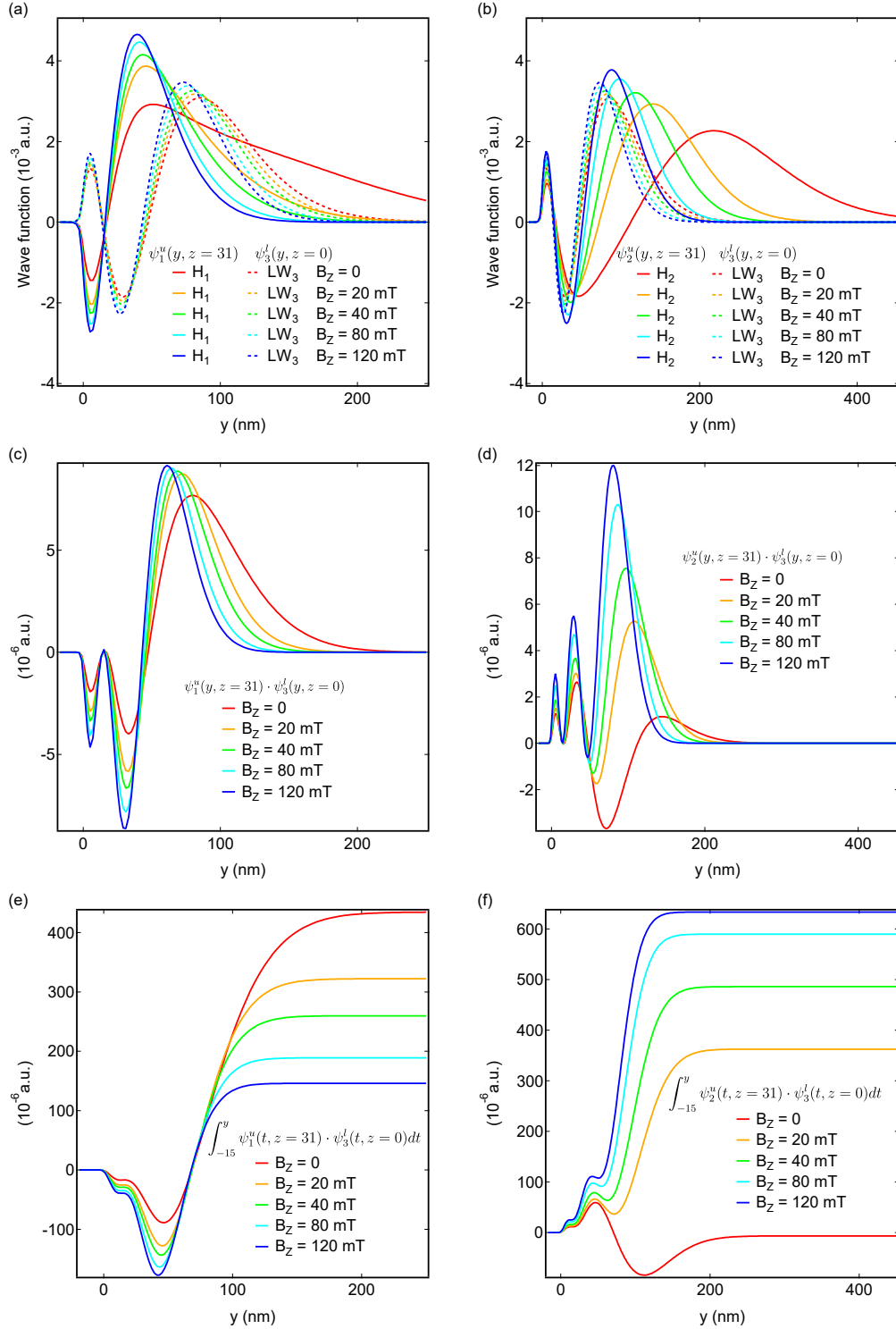


FIG. S9. (a) The cross section along the y -direction of the wave functions of hybrid state H_1 in the upper system ($z = 31$ nm) and wire mode LW_3 ($z = 0$) in the lower system at several magnetic fields B_Z . (b) Similar to (a) but for state H_2 in the upper system. (c,d) The product of upper system and lower system wave function cross sections from panels (a) and (b), respectively. (e,f) The result of integration of the products from panels (c) and (d). All position coordinates are given in nanometers.

IV. EXCEPTION FROM THE SELECTION RULE

There are some exceptions from this rule, which can be explained by a dominant contribution to the overlap from the outermost lobes, those most removed from the hard wall of the cleaved edge. Due to the quasi-triangular shape of the confinement potential, the outermost lobes of the wave function have by far the most weight. This is the case for the tunneling resonance $H_1 - LW_3$, shown in the left column of Fig. 3 in the main text. The selection rule predicts a weak tunneling conductance at zero field, as the number of lobes in the tunneling region (dashed box) is different for upper and lower wells. However, the actual overlap between these two wave functions is strong. This is due to the large overlap between the two last lobes, which overpowers the negative contributions from the other lobes. As the magnetic field B_Z increases, the magnetic compression of the edge states reduces the width of the last lobe and the selection rule holds again.

V. HYBRIDIZATION

The background conductance during the measurement shown in Fig. 5 of the main text was suppressed by reducing the size of the source region to $22\ \mu\text{m}$ using another surface gate. This gives weak parallel replicas of observed resonances, likely originating from a nonuniform density in the source region.

The tunneling conductance measured also for the negative values of magnetic field B_Z is shown in Fig. S10. The direction of edge state propagation is reversed for negative B_Z and the dispersion relation is mirrored on the vertical axis (see left insets). As a result, the resonance that tracks the wire-like states for one sign of B_Z will track the avoided crossings for the opposite sign of B_Z .

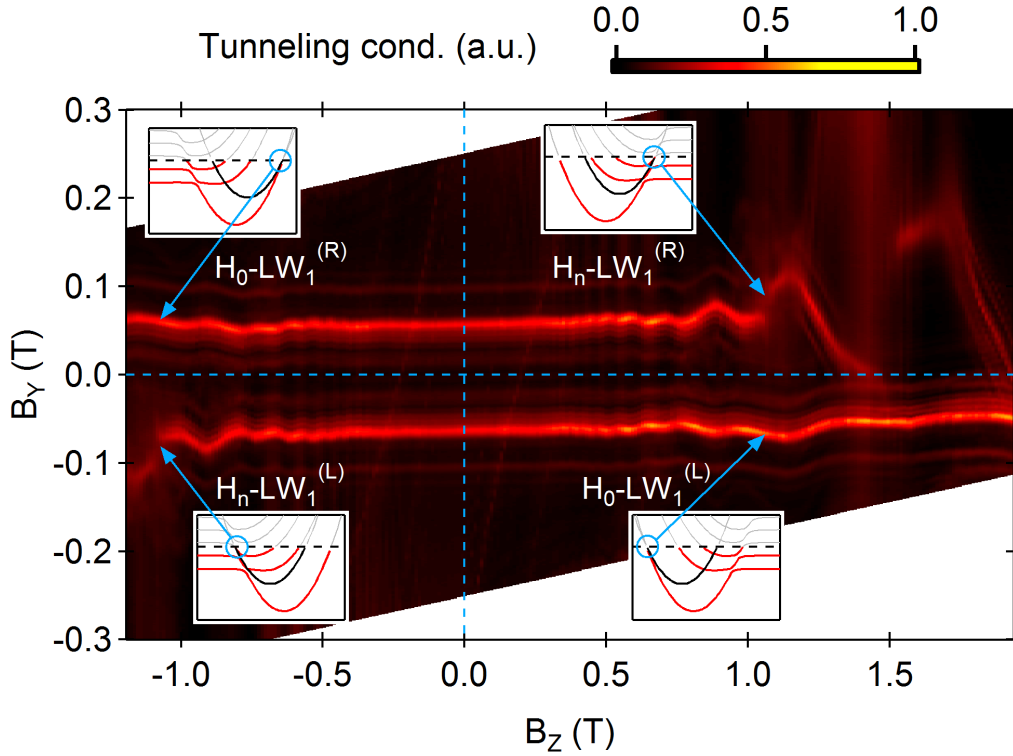


FIG. S10. Tunneling conductance between hybrid states in the upper system and the lower wire mode LW_1 . Insets qualitatively depict the dispersion relation of the hybrid states (red) and LW_1 (black) for B_Y and B_Z which satisfy the resonant tunneling condition.

VI. ELECTRON DENSITY PROFILES

The density profile of the hybrid states, shown in Fig. S11a), as well as the total electron density, shown in Fig. S11b), can be constructed from the wave functions by integrating over the momenta and z . Sufficiently far away from the edge, the hybrid states reach the bulk Landau level density, as expected. Close to the edge, a strong overshoot in density appears, due to the triangular wire confinement potential giving extra charges predominantly in H_0 . The subsequent oscillations of density, most pronounced for H_0 , are caused by the potentials forming an effective barrier between two minima.

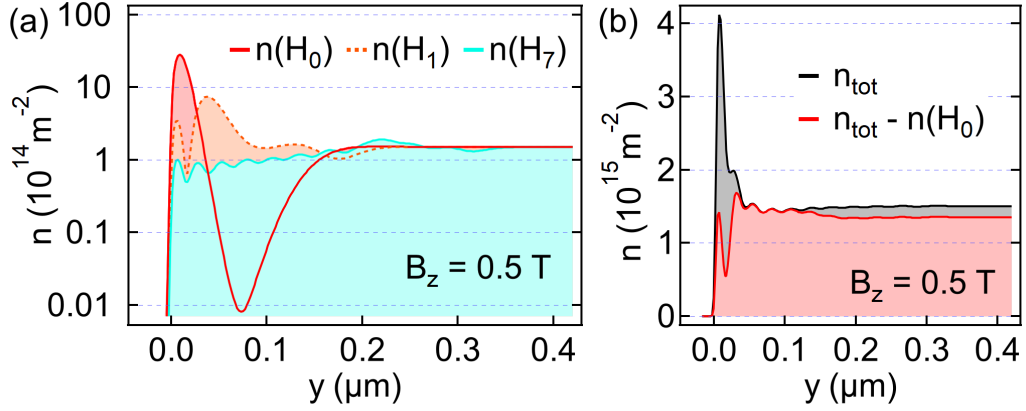


FIG. S11. (a) Electron density of several hybrid states as well as (b) the total electron density with (black) and without (red) the contribution from H_0 , as a function of distance y from the cleavage plane, on the same horizontal scale as Fig. 4(b) of the main text.

VII. NUMERICAL CALCULATIONS

The schematic diagram of the $y-z$ cross section of the sample used in this study is shown in the Fig. S12 (not to scale). The Fermi level was pinned to mid gap on the surface of GaAs cap layers (top and left surfaces in Fig. S12). The electric field in the bulk of the sample along the y and z axes was assumed to be zero due to charge neutrality (right and bottom surfaces). Using these boundary conditions, we self-consistently calculated the conduction band for the interior of the sample, $V(y, z)$. The Schrödinger equation was solved in the quantum region that includes both quantum wells and tunnel barrier between them. The origin of the z axis was placed in the center of the lower quantum well. We used the vector potential $\mathbf{A} = (zB_Y - yB_Z, 0, 0)$ to write the down the Hamiltonian:

$$H = \frac{p_Y^2 + p_Z^2}{2m} + \frac{(\hbar k_X - ezB_Y + eyB_Z)^2}{2m} + V(y, z) \quad (\text{S1})$$

To calculate the position and strength of tunneling resonances, we split the system into two parts, one with the upper and one with the lower quantum well. The position of the tunneling resonance $H_n - LW_m$ for any given magnetic field B_Z was found by iteratively changing the momenta k_x and magnetic field B_Y to match the energy of these two states with the Fermi level. This procedure was repeated for all the resonances over a range of B_Z for the calculations shown in the right panel in Fig.2 of the main text. The coarse grid (10 nm in the y -direction, 2.5 nm in the quantum wells and 1 nm in the tunnel barrier in the z -direction) was used to speed up the calculations process. We checked for several resonances at multiple magnetic field values B_Z that the overlaps calculated using the fine grid (2 nm in the y -direction, 1 nm in the quantum wells and 1 nm in the tunnel barrier in the z -direction) deviate no more than 20% from the values obtained using the coarse grid in case of substantial overlap.

The conduction band profiles and the wave functions shown here and in the main text were calculated using the grid with the intermediate resolution (2 nm in the y -direction, 2 nm in the quantum wells and 1 nm in the tunnel barrier in the z -direction).

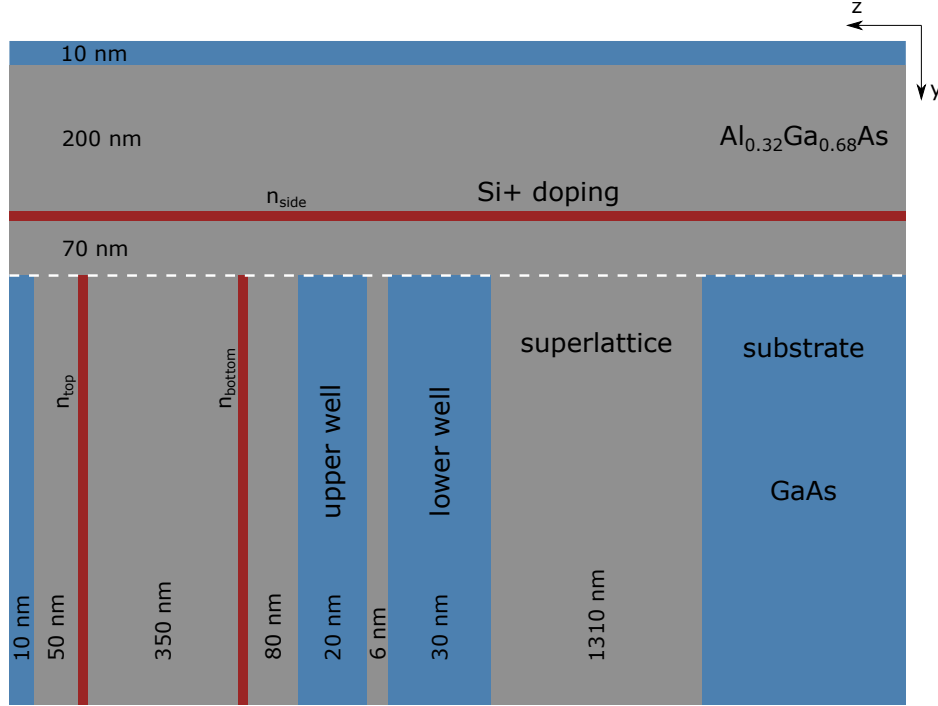


FIG. S12. Schematic diagram of the GaAs/AlGaAs cleaved edge overgrowth double quantum well heterostructure. The density of the ionized dopants was tuned to give the best match with the positions of the various fans in Fig. 2 of the main manuscript, resulting in $n_{top} = 3.2 \times 10^{11} \text{cm}^{-2}$, $n_{bottom} = 2.6 \times 10^{11} \text{cm}^{-2}$ and $n_{side} = 3.2 \times 10^{11} \text{cm}^{-2}$.

-
- [1] C. P. Scheller, S. Heizmann, K. Bedner, D. Giss, M. Meschke, D. M. Zumbühl, J. D. Zimmerman, and A. C. Gossard, *Applied Physics Letters* **104**, 211106 (2014).
 - [2] D. E. F. Biesinger, C. P. Scheller, B. Braunecker, J. Zimmerman, A. C. Gossard, and D. M. Zumbühl, *Phys. Rev. Lett.* **115**, 106804 (2015).
 - [3] D. Maradan, L. Casparis, T.-M. Liu, D. E. F. Biesinger, C. P. Scheller, D. M. Zumbühl, J. D. Zimmerman, and A. C. Gossard, *J. Low. Temp. Phys.* **175**, 784 (2014).
 - [4] T. Patlatiuk, C. P. Scheller, D. Hill, Y. Tserkovnyak, G. Barak, A. Yacoby, L. N. Pfeiffer, K. W. West, and D. M. Zumbühl, *Nature Communications* **9**, 3692 (2018).